Original Research

Influences of blood flow parameters on temperature distribution during liver tumor microwave ablation

Jinying Wang[1], Shuicai Wu[1], Zeyi Wu[1], Hongjian Gao[1,*], Shengyang Huang[1,*]

[1]*Faculty of Environmental and Life Sciences, Beijing University of Technology, 100124 Beijing, China*

TABLE OF CONTENTS

1. Abstract

Highlights: (1) A 3D simulation model of MWA (microwave ablation) based on the temperature-dependent characteristic parameters and blood flow parameters was established to realize the visual simulation of temperature distribution and coagulation zone. The internal forced convection condition was used to accurately characterize the large vessel. (2) The *ex vivo* MWA experimental platform was built to verify the accuracy of the simulation model. A peristaltic pump was employed for operatively controlling blood circulation and a medical soft plastic tube was introduced for appropriately simulating a blood vessel. (3) The influences of blood flow parameters of large vessels on temperature distribution and coagulation zone were systematically analyzed in order to provide reference and guidance for MWA clinicians. **Purpose**: Clinical MWA of liver tumor is significantly limited by the accurate prediction of vascular cooling effects. To provide reference and guidance for clinical MWA of liver tumor, the three-dimensional effects of different blood flow parameters of large vessels on MWA temperature distribution were systematically evaluated. **Materials and methods**: Firstly, the MWA three-dimensional finite element simulation model with blood flow parameters was established. Secondly, to verify the effectiveness of the model, MWA was performed *ex vivo* in porcine liver for 360 s and the temperature was measured by thermocouples. A medical soft plastic tube was placed parallel to the MWA antenna to simulate a natural liver vessel. Finally, based on this model, the influences of different vessel diameters and vessel-antenna spacings on MWA temperature distribution were analyzed. **Results**: Sixteen ablations were performed to verify the accuracy of the simulation model. The mean temperature errors between measured data and simulation results at six measurement points were 3.87 °C. In the first 10 seconds of MWA, the vessel cooling effect on temperature distribution was negligible. When the vessel-antenna spacing was 5 mm and the vessel diameter varied from 3 mm to 6 mm, the temperature at the measured point near the vessel decreased by 2.11 °C at 360 s. When the vessel diameter was 6 mm and the vessel-

Submitted: 15 July 2021 Revised: 20 August 2021 Accepted: 26 August 2021 Published: 30 September 2021

antenna spacing varied from 5 mm to 7 mm, the temperature at the measured point near the vessel reduced by 14.91 °C at 360 s. In addition, blood diameter had little influence on the temperature distribution near the heating point. The volume of coagulation zone will not be obviously affected once the vessel lies outside the predicted coagulation zone. **Conclusions**: The MWA simulation model with blood flow parameters is established. Vessel-antenna spacing is the primary factor affecting the temperature distribution. A vessel with larger diameter can have a more significant effect on the temperature distribution. The large vessel will take away and block part of conduction heat, so the coagulation zone will not be formed on the lateral side of the vessel.

2. Introduction

Thermal ablation is an alternative to traditional surgical treatment, radiotherapy, chemotherapy and immunotherapy. It is more and more favored by clinical experts and researchers because of its advantages of less damage to patients and rapid postoperative recovery [1, 2]. Moreover, thermal ablation is very effective for primary and secondary liver tumors [3]. The principle is to achieve the tumor necrosis by heating the tissue [4]. Compared with radiofrequency ablation (RFA) [5], MWA has the advantages of larger coagulation zone, uniform heating, and no need of electrode patch, which has attracted more and more attention [6–8].

MWA preoperative plan for liver tumor mainly includes the following steps: firstly, the three-dimensional reconstruction is carried out through medical images, and the thermal ablation temperature of tumor is simulated. Finally, the treatment parameters such as heating time, MWA power and needle trajectory are planned. After the operation, medical imaging is used to evaluate the postoperative effects. In the above process, building the real temperature simulation model is the technical challenge in this field [9], and it is also the key to improve the surgical effects.

Huang *et al*. [10] explored the influences of the blood flow characteristics of a single vessel and a pair of parallel convection vessels with the diameter of 1 mm and 2 mm on the coagulation zone when they were orthogonal or parallel to the antenna. Although convective heat conduction was considered, the Nusselt number and microstructure parameters were fixed. Also, the temperature dependences of these parameters were ignored. Vaidya *et al*. [11] studied the influences of blood coagulation effect of vessels less than 1 mm in diameter on the ablation results during MWA. The direction of blood flow in the 0.4 mm–0.5 mm vessel had the most significant effect on the coagulation zone. However, the experiments relating to large vessels were not involved. Chen *et al*. [12] analyzed the temperature distribution characteristics during RFA for the heat sink effects of large vessels. Based on the simplified Pennes bioheat equation, the weighted temperature field was obtained to minimize the interference caused by microvascular perfusion effect. This study did not consider the small differences caused by different vascular systems when simulating the cooling effects of large vessels. Lu *et al*. [13] used a Y-shaped copper tube to study the influences of blood flow of bifurcation vessel and different spacings from microwave antenna on temperature field. The simulation model of temperature distribution was established by omitting electromagnetic simulation calculation through measured SAR (specific absorption rate). The 54 °C isotherm surface was used to describe the influences of blood flow, vessel position and spacing on coagulation zone. However, the experiment only obtained a planar temperature field, which could not reflect the influences of blood vessels on the temperature distribution in three-dimensional space. Chen *et al*. [14] simulated the dynamic temperature distribution and determined the optimal input power by controlling the maximum temperature of RFA. It was found that the blood vessels parallel to the RF (radio frequency) antenna would bring more heat loss than the orthogonal ones. The diameter of the blood vessel, the spacing from the antenna and the heating power are the main factors affecting the ablation temperature distribution.

To sum up, there still are few systematic studies on the heat dissipation of large vessels [15, 16] with diameter of 3 mm and above [17, 18]. Previous studies are limited by the accuracy of the simulation model, and mainly focus on the small vessels with diameter less than 2 mm, so cannot meet the clinical needs.

This work aims to study the impact of large vessels on the temperature distribution and the coagulation zone during MWA, particularly focusing on (i) building the MWA temperature simulation model, which includes blood flow characteristics (vessel diameter, blood flow velocity and vessel-antenna spacing); (ii) verifying the accuracy of the simulation model by *ex vivo* MWA experiments, and finally (iii) analyzing the effects of different blood flow parameters on the temperature distribution and the coagulation zone during MWA. This study can provide an important reference for clinical MWA preoperative planning and improve the quality of surgical ablation.

3. Materials and methods

3.1 Experimental setup

The experimental system includes a cooled-shaft MWA device (KY-2000; Kangyou Microwave Energy Sources Institute, Nanjing, China), a microwave antenna, metallic thermometers (YWY-2, Kangyou Microwave Energy Sources Institute, Nanjing, China), *ex vivo* porcine livers, a peristaltic pump for blood circulation (S100(300)-2B+mYZ15; Baoding Ditron Technology Co., Ltd., Baoding, China), a medical soft plastic tube for simulating a blood vessel (Fig. 1).

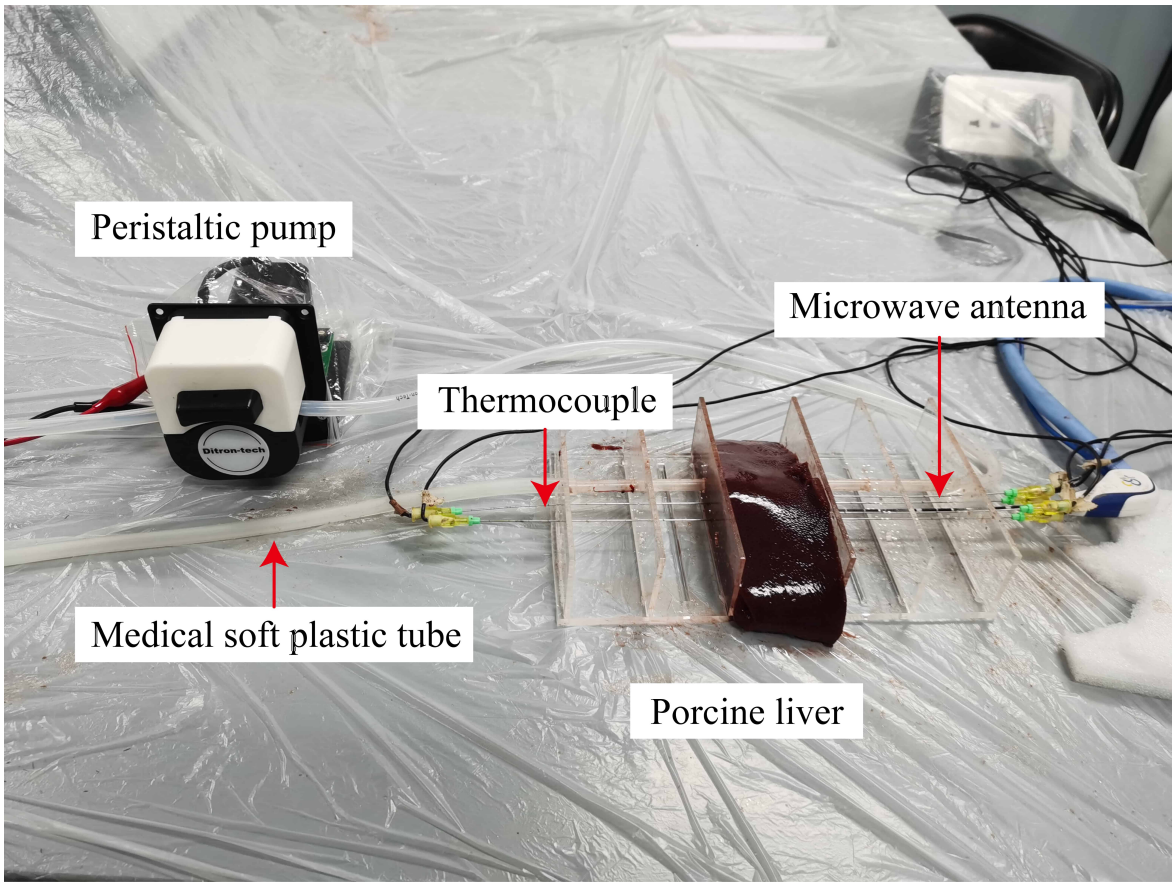

Fig. 1. ***Ex vivo*** **experiment platform for microwave ablation.**

The MWA device equipped with thermometers can display the temperature changes in real time and save the collected temperature data automatically. The water-cooled antenna used in the MWA experiments works at 2450-MHz. The diameter of the thermometer is 1 mm and the length is 120 mm. The effective measurement point is located at the tip of the thermometer, and the measurement accuracy is 0.1 °C. The outer diameter of the medical soft plastic tube used to simulate the large vessel is 6 mm. In order to simplify the calculation, the tube wall thickness is ignored.

Fresh porcine liver was used to replace human liver tumor tissue. Purified water was used to replace blood. The experiment was performed at 15 °C. The initial temperature of both the porcine liver and purified water used in the experiment was about 15 °C. A peristaltic pump was employed to control the flow rate in the medical soft plastic tube accurately. The flow range of the peristaltic pump was 0.0048 mL/min–620 mL/min. According to the diameter of medical tube and the average flow rate of human liver blood vessel (0.2 m/s) [10], the flow rate of peristaltic pump was adjusted to 340 mL/min.

3.2 Modeling of MWA temperature distribution

Since the three-dimensional effects of blood flow parameters on temperature distribution cannot be obtained by MWA *ex vivo* experiments, a 3D simulation model was established by COMSOL software (version.5.5; COMSOL Inc, Stockholm, Sweden) to evaluate the cooling effects of blood vessels systematically. Firstly, a cylindrical liver tumor model with a radius of 50 mm and a height of 100 mm was constructed (Fig. 2). A microwave antenna was inserted longitudinally at the center of the bottom circle, and a cylindrical tube parallel to the MWA antenna was included as a blood vessel. In this model, the vessel radius and the vessel-antenna spacing can be adjusted appropriately. After the geometric model was built, the automatic meshing method was used to mesh the model. It took about 30 min to solve once.

The MWA finite element simulation model was solved by the coupling of electromagnetic field and bioheat field. The classical Pennes bioheat equation was used to solve the bioheat problem in COMSOL [19] because of its simplicity and convenience. The expression of the equation is as follows:

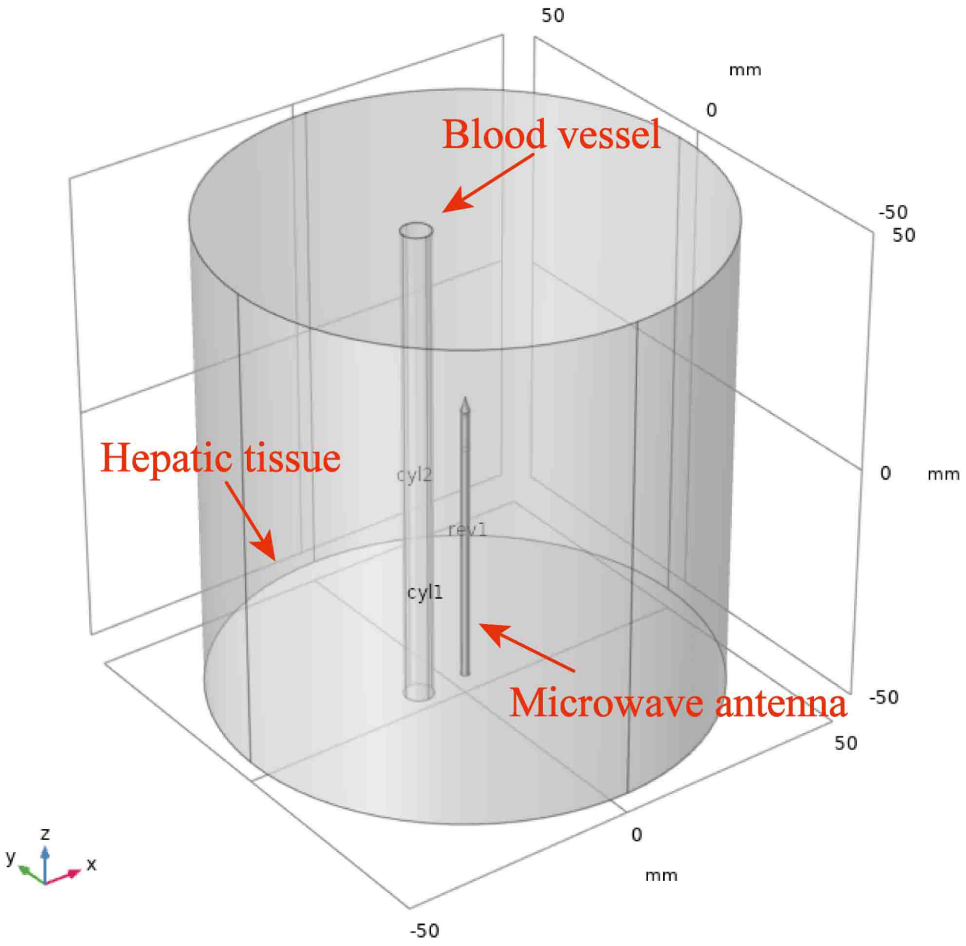

Fig. 2. Geometric model of MWA simulation.

$$\rho \cdot Cp \cdot \frac{\partial T}{\partial t} + \nabla \cdot (-k\nabla T) = \rho_b c_b \omega_b (T_b - T) + Q_{\text{met}} + Q_{\text{ext}} \quad (1)$$

where ρ represents the tissue density (kg/m^3), Cp represents the specific heat capacity of the tissue $(J/(kg \cdot K))$, is the thermal conductivity of the tissue $(W/(m \cdot K))$, T is the tissue temperature $(^{\circ}C)$, ω_b is the blood perfusion rate $(kg/m^3 \cdot s)$, Q_{met} and Q_{ext} $\left(W/m^3\right)$ are the heat produced by tissue metabolism and microwave antenna. The subscript *'b'* represents the characteristics of blood.

In order to characterize the heat transfer between blood vessel and tissue, the internal forced convection heat transfer condition was set in COMSOL to simulate the influences of large vessels on the temperature distribution and coagulation zone [20]. The heat transfer between blood vessel and tissue can be described by Newton formula [21]:

$$-n \cdot (-k\nabla T)(x,t)) = h_b (T_{\text{b}} - T(x,t)) \quad (2)$$

where h_b stands for the heat transfer coefficient. Under the condition of constant blood flow, the above formula can be simplified as [22, 23]:

$$h_b = Nu_D K_b / D \quad (3)$$

where Nu_D is the local Nusselt number, K_b is the thermal conductivity of blood vessel $(W/(m{\cdot}K))$, D is the diameter of blood vessel (m).

$$Nu_D = 4 + 0.48624\,\text{In}^2[\text{Re} \cdot \text{Pr} \cdot D/(18 \cdot L)] \quad (4)$$

$$\text{Re} = \rho_b V_b D/\mu \quad (5)$$

$$\text{Pr} = \frac{Cp \cdot \mu}{\lambda} \quad (6)$$

where Re is Reynolds number, and Pr is Prandtl number, L is the vascular length (m), λ is the thermal conductivity $(W/(m{\cdot}K))$, $V(m/s)$ and $\mu(mPa{\cdot}s)$ stand for the average blood flow rate and the blood viscosity [24]. Based on vessel diameter and blood flow rate, the heat transfer between blood vessel and tissue can be automatically calculated.

Table 1. The values of characteristic parameters of *ex vivo* porcine liver at 25 °C.

Tissue	$\rho_(kg/m^3)$	$Cp_(J/(kg\cdot K))$	$k(W/(m\cdot K))$	$\sigma_{(S/m)}$	$\mathcal{E}$
porcine liver	1050	3628	0.565	1.8	44.3

The values of characteristic parameters of *ex vivo* porcine liver at 25 °C are listed in Table 1. During MWA, the thermal and electrical parameters of liver tissue can vary with the increase of temperature. In order to describe the real variation of these parameters, the temperature-dependent electrical parameters, the specific heat capacity function based on water content variation and the thermal conductivity function with linear variation were used in this study [25].

The specific heat capacity function based on the change of water content is as follows [26–28]:

$$Cp(T) = \begin{cases} Cp_{\text{at 25 °C}} + k_c \cdot (T-25) & T \le 70\ ^\circ\text{C} \\ Cp_{\text{at 70 °C}} - \frac{\alpha}{\rho} \cdot \frac{\partial W(T)}{\partial T} & T > 70\ ^\circ\text{C} \end{cases} \quad (7)$$

$$W(T) = \begin{cases} 0.778 \cdot \left(1 - \exp\left(\frac{T-106}{3.420}\right)\right) & 70\ ^\circ\text{C} \le T < 100\ ^\circ\text{C} \\ 7.053 - 0.0640 \cdot T & 100\ ^\circ\text{C} \le T < 104\ ^\circ\text{C} \\ 0.778 \cdot \exp\left(-\frac{T-80}{34.370}\right) & 104\ ^\circ\text{C} \le T \end{cases} \quad (8)$$

where $Cp_{\text{at 25 °C}}$ and $Cp_{\text{at70 °C}}$ represent the specific heat capacities at 25 °C and 70 °C, respectively; k_c represents tissue water density; α represents the latent heat constant (set to 2260 kJ/kg).

Based on references [28–30], the expressions of relative permittivity conductivity σ, and thermal conductivity k are as follows:

$$\varepsilon(T) = 45 \cdot \left[1 - \frac{1}{1 + \exp(5.200 - 0.0519 \cdot T)}\right] \quad (9)$$

$$\sigma(T) = 2.2 \cdot \left[1 - \frac{1}{1 + \exp(5.324 - 0.0607 \cdot T)}\right] \quad (10)$$

$$K(T) = K_{at25^\circ\text{C}} + 0.00111 \cdot (T-25) \quad (11)$$

Denaturation will occur in a short time when the liver tissue is between 50 °C and 60 °C [31]. In this study, the degree of tumor necrosis based on 54 °C threshold [32, 33] was used to evaluate and characterize the size of coagulation zone (Fig. 3).

3.3 Model validating based on MWA experimental results of porcine liver *ex vivo*

In MWA experiments, an acrylic mold with 12 cm long, 5 cm wide and 4.5 cm high was designed to house porcine liver. The microwave antenna was placed in the center of porcine liver tissue, and a medical soft plastic tube with a diameter of 6 mm was inserted 10 mm away from the antenna as a simulated large blood vessel. Six temperature measuring points (CH_1(5, 0, 3), CH_2(–5, –5, 0), CH_3(5, –5, 0), CH_4(–5, 0, 3), CH_5(–5, 0, 12), CH_6(5, 0, 12)) were selected. They were symmetrically distributed on both sides of the antenna The heating point of the microwave antenna was taken as the coordinate origin. The points CH_2, CH_4 and CH_5 were set near the blood vessel side. Before MWA, the peristaltic pump was started to ensure smooth water circulation. The microwave heating power and the heating time were set to 60 W and 360 s, respectively. Sixteen groups of experiments were carried out and eleven groups of effective data were obtained. The average temperature at each temperature measuring point was taken as the experimental data.

In order to further verify the consistency between the simulation results and the MWA data *ex vivo*, the size of coagulation zone was measured. After the thermal ablation experiments, the porcine liver was cut horizontally along the microwave antenna, and the shape and area of the coagulation zone were observed and measured.

3.4 Evaluating the effects of vessel diameter and vessel-antenna spacing on temperature distribution in MWA

Blood vessels with diameter less than 3 mm or even less than 1 mm have been deeply studied [10, 11]. During MWA, small blood vessels close to the antenna are prone to blood coagulation, which may damage the vessel wall. For vessels with larger diameter, the blood will cool and protect the large vessels from heating damage. In this case, the temperature distribution of MWA needs to be further explored.

Therefore, this study focuses on the influences of vessels with diameters of 3 mm and 6 mm on the temperature distribution during MWA. The vessel-antenna spacing starts from 5 mm and increases by 2 mm each time. Six assessment points (P_1(–5, 0, 0), P_2(–5, 0, 5), P_3(–5, 0, –5), P_4(–3, 0, 0), P_5(–3, 0, 10), P_6(–3, 0, -10)) were set. They were selected in the FEM (finite element method) model to analyze the influences of vessel diameter and vessel-antenna spacing on temperature distribution.

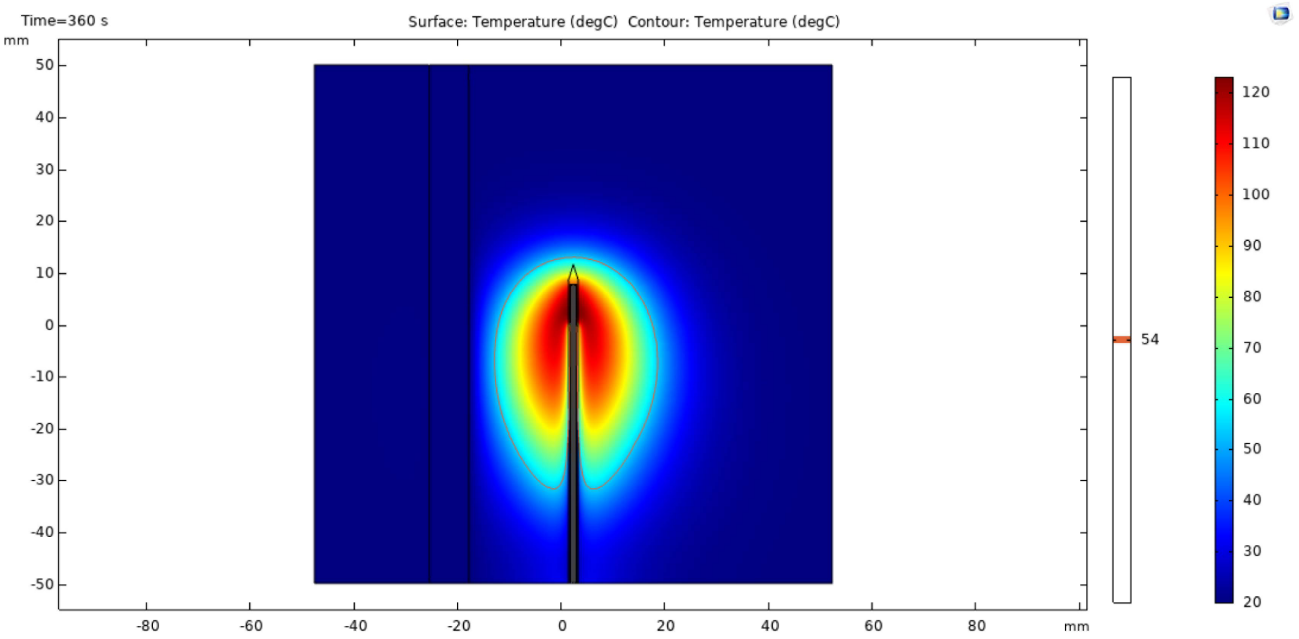

Fig. 3. Schematic diagram of 54 °C isothermal surface of MWA.

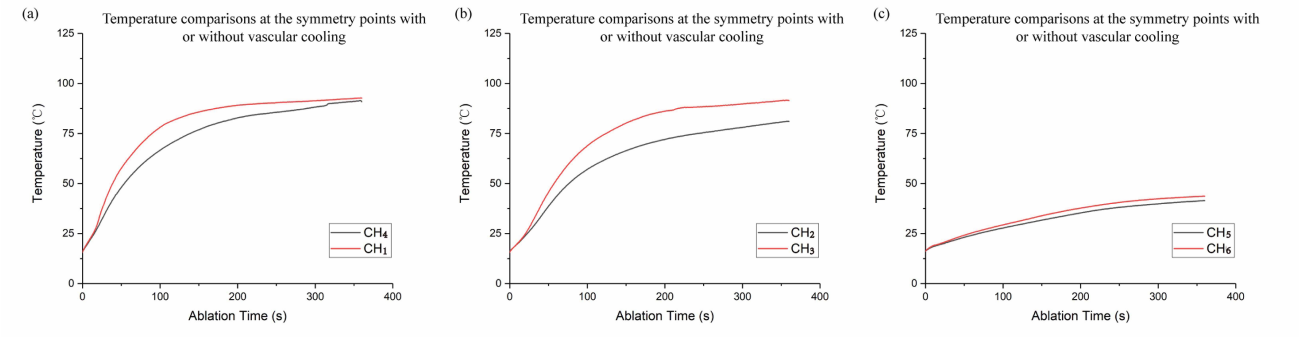

Fig. 4. Temperature comparisons at the symmetry points. The gray and red curves represent the temperature changes at the temperature measuring points with and without vascular cooling, respectively. (a) shows temperature comparisons at CH_4 and CH_1, (b) shows temperature comparisons at CH_2 and CH_3, and (c) shows temperature comparisons at CH_5 and CH_6.

4. Results

4.1 MWA results of porcine liver *ex vivo*

Eleven groups of effective data were collected from CH_1–CH_4, and 4 groups were collected from CH_5 and CH_6. The average of each group of experimental data was used as the real temperature profile. Fig. 4 shows the temperature comparisons of three groups of symmetrical temperature measuring points (CH_1 vs. CH_4, CH_2 vs. CH_3, CH_5 vs. CH_6).

CH_1 and CH_3 were closer to the heating point of microwave antenna, and there was no blood vessel at this side. They exhibited faster heating rates and higher tissue temperatures after heating. In contrast, the overall heating rates and final temperatures at CH_2 and CH_4 on the opposite side of CH_3 and CH_1 were lower due to the influences of blood flow. It was found that the cooling effects of blood vessels on temperature at CH_5 and CH_6 were less obvious. It was apparent that the temperature rising speeds and final temperatures at CH_2, CH_4 and CH_5 (on the cooling side) were lower than those at the corresponding points CH_3, CH_1 and CH_6.

CH_5 and CH_6 were far away from the heating point, which leaded to the lower maximum temperatures at these two points. CH_5 was much further away from the vessel, thus the cooling effect of the blood vessel at CH_5 was not as obvious as CH_2 and CH_4. This explains why the temperatures at 360 s of CH_5 and CH_6 were lower and the temperature difference was much smaller than other two groups of temperatures.

Table 2. Comparisons of coagulation zone sizes between *ex vivo* experiments and simulations (in millimeters).

	Group 1	Group 2	Group 3	Group 4	Group 5	Mean	Simulation	Error
Long axis	40	40	42	42	40	40.8	39	1.8
Short axis	17	18	23	22	23	20.6	22	–1.4

4.2 Validation of finite element simulation model based on measured data

4.2.1 Experimental validation of simulated temperature distribution

The mean temperature of the same measurement point was taken as the result of *ex vivo* experiment, and the result was compared with simulation data to verify the effectiveness of the simulation model (Fig. 5).

The measured data and simulation data of each measurement point had substantially the same temperature rising trends. The mean errors between the experimental and simulated temperatures at CH_1, CH_3 and CH_6 were 3.17 °C, 4.95 °C and 7.83 °C, respectively. The mean errors between the experimental and simulated temperatures at CH_2, CH_4 and CH_5 (on the cooling side) were –2.89 °C, 1.37 °C and 2.97 °C, respectively. According to the temperature measurements of the 6 points above, the mean temperature errors between measured data and simulation results were 3.87 °C. The simulation data were in good agreement with the results of the *ex vivo* experiments. Therefore, the simulation model can be used to obtain the effects of blood flow parameters and improve the ablation efficiency.

4.2.2 Validation of coagulation zone size

After microwave ablation, the porcine liver tissues were cut horizontally along the antenna insertion direction, as shown in Fig. 6. It can be clearly seen that the coagulation zone includes carbonization zone, coagulation zone and ablation transition zone [31]. The black area is the carbonization zone, the gray area is the coagulation zone, and the outermost light red area is the ablation transition zone.

The results showed that the coagulation zone on the blood cooling side was smaller than that on the other side. The sizes of the coagulation zones of *ex vivo* experiments and simulations are shown in Table 2. The long axis error was 1.8 mm and the short axis error was –1.4 mm, which can further verify the effectiveness of the simulation model.

4.3 Effects of vessel diameter and antenna-vessel spacing on the MWA results

It can be seen from Fig. 7 that the changes of vessel diameter and vessel-antenna spacing will affect the temperature distribution of MWA. Under the condition of only changing the spacing (from 5 mm to 7 mm), the temperature at 360 s of P_1, P_4 and P_6 decreased by 14.4%, 3.3% and 5.1%, respectively. The temperature of P_1 decreased most significantly because it was closest to the blood vessel. P_4 and P_6 had the same vessel-antenna spacing, however P_4 is closer to the heating point, so the temperature at this point decreased less obviously than that at P_6. This clearly showed the significant influences of vessel-antenna spacing on temperature distribution. In the case of only changing the diameter of the blood vessel (from 3 mm to 5 mm), the temperature at 360 s of P_1, P_4 and P_6 decreased by 2.4%, 0.9% and 1.3%, respectively. This indicated that the diameter of the blood vessel had little effects on temperature distribution of MWA.

By changing the vessel diameter and the vessel-antenna spacing, the temperature varied obviously and different volume of coagulation zone was obtained. However, no coagulation zone was observed on the lateral side of the vessel (Fig. 7) in all cases.

When the ablation time is less than 10 s, the microwave energy deposition plays a dominant role [34]. Paired *T*-test was carried out on the temperature data of the first 10 seconds under different blood flow conditions. The results showed that all the *P* values were greater than 0.05, so there was no significant difference. Therefore, the cooling effects of large vessel could be ignored in the first 10 seconds of MWA, which was capable to simplify treatment planning of some short MWA procedures. As the ablation time elapsed, the temperature differences under different blood flow conditions began to increase, until the end of the ablation (at 360 s), the differences reached the maximum (Tables 3,4).

Fig. 8 shows the influences of blood flow parameters on the coagulation zone. The coagulation volume after 360 s MWA were 26410 mm^3, 25934 mm^3, 23594 mm^3 and 22000 mm^3in four groups of simulations under different conditions (S_1: d = 3 mm, D = 17 mm; S_2: d = 6 mm, D = 17 mm; S_3: d = 3 mm, D = 5 mm; S_4: d = 6 mm, D = 5 mm. d stands for the vessel diameter, D stands for the vessel-antenna spacing and the blood flow rate was 2.0 m/s). When the vessel diameter changed from 3 mm to 6 mm, the volume of coagulation zone was reduced by 1.8% (S_1 vs. S_2; vessel-antenna spacing = 17 mm) and 6.8% (S_3 vs. S_4; vessel-antenna spacing = 5 mm), respectively. In the case of smaller vessel-antenna spacing, the change of vessel diameter had a greater impact. When the vessel-antenna spacing changed from 17 mm to 5 mm, the volume of coagulation zone decreased by 10.7% (S_1 vs. S_3; vessel diameter = 3 mm) and 16.7% (S_2 vs. S_4; vessel diameter = 5 mm), respectively. In the case of larger vessel diameter, the effect of changing the vessel-antenna spacing was greater. Through data analysis, it could be seen intuitively that vessel-antenna spacing had a greater influence on the coagulation zone than vessel diameter.

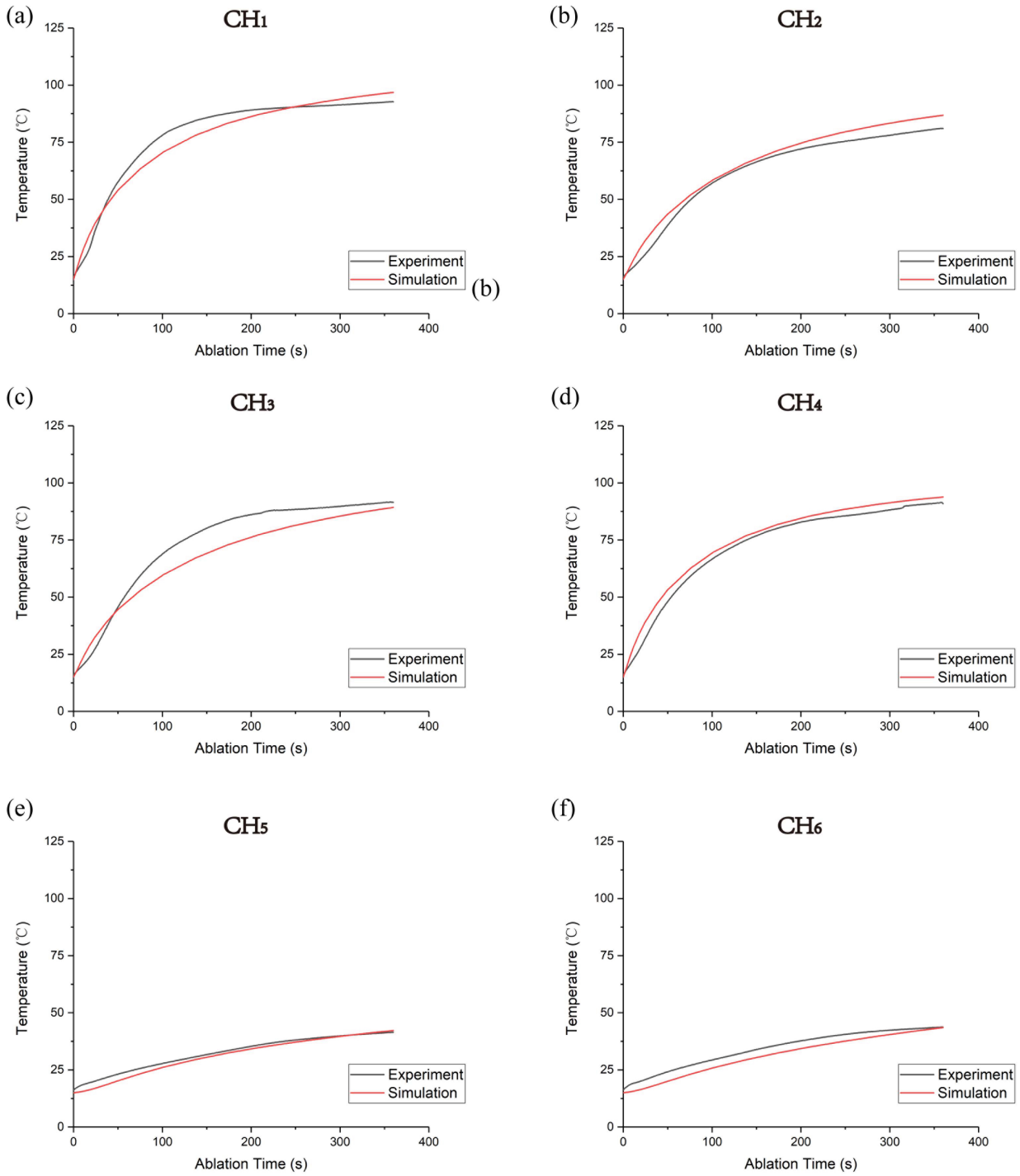

Fig. 5. Comparisons between thermal ablation data and simulation results at (a) the measurement point CH_1, (b) the measurement point CH_2, (c) the measurement point CH_3, (d) the measurement point CH_4, (e) the measurement point CH_5, (f) the measurement point CH_6.

In order to further learn the significant influences of vessel-antenna spacing on coagulation zone, the vessel-antenna spacing was continually changed. Several different distances (D = 5 mm, D = 17 mm, D = 18 mm, D = 20 mm) were selected for simulation, where the vessel diameter was 3 mm, and the blood flow rate was 0.2 m/s. It was found that when the distance between the vessel and the antenna exceeds the predicted length of the short half axis (about 17 mm), the influences of the vessel on the coagulation zone volume are limited (0.7%, 1.2%, 1.7%). Therefore, in MWA, it was believed that if the blood vessel was located outside the simulation coagulation zone, the coag-

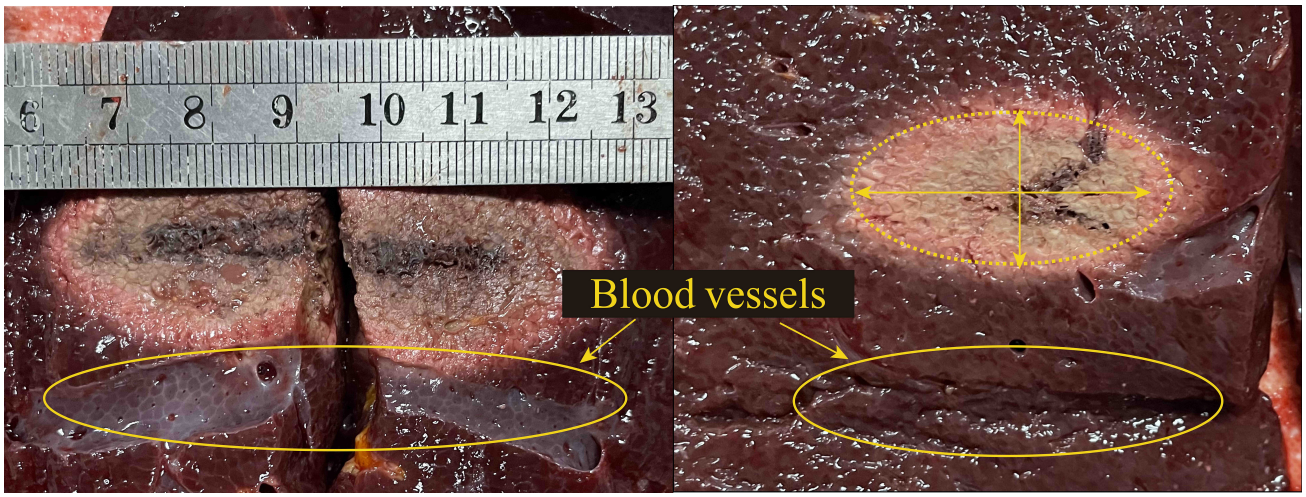

Fig. 6. Profile of coagulation zone of porcine liver after MWA (the diameter of blood vessels was 6 mm, the antenna-vessel spacing was 10 mm). Abbreviation: MWA, microwave ablation.

Table 3. The temperature difference for vessel-antenna spacings of 7 mm and 5 mm in the case of vessel diameter of 6 mm.

	P_1 [95% CI*]	P_4 [95% CI*]	P_6 [95% CI*]
Mean temperature difference during first 10 s	0.49 [0.16–0.82]	1.07 [0.80–1.34]	0.06 [0.02–0.10]
Temperature difference at 360 s	14.91	3.83	5.23

*95% CI denotes Confidence interval at 95% confidence level.

ulation zone could hardly be affected by the vessel. Thus, the changes of the characteristic length and the coagulation zone shape could be ignored. This is mainly due to MWA is not sensitive to heat-sink effect compared with RFA [35].

5. Discussion

With the development of tumor thermal ablation technology, some methods are possible to detect the ablation temperature. CT (computed tomography) [36], US (ultrasound) [37, 38], HIFU (high intensity focused ultrasound) [39] and MRI (magnetic resonance imaging) [40] are employed alone or in combination to monitor the ablation procedure noninvasively. Based on attenuation values from noninvasive CT Thermography, tissue temperature can be accurately predicted during thermoablation [36]. A major challenge of US noninvasive monitoring is to separate the apparent displacement caused by thermal effect from the real tissue motion independent of heating [37]. In addition, US noninvasive monitoring is easily affected by motion artifacts [38]. MRI can quantify the temperature by using a temperature sensitive MR contrast agent [40], but the process is expensive and cumbersome. These methods rely largely on the quality of intraoperative and postoperative images.For the thermal ablation of the tumor near large vessels, not only accurate monitoring, but also preoperative simulation is needed to ensure the operation effects. The previous studies [10, 11] on small vessels (diameter less than 3 mm) cannot meet the clinical MWA requirements. Therefore, a 3D temperature simulation model based on the flow characteristics of large vessels was established. The model can accurately simulate an *ex vivo* setting, directly present the volume and shape of coagulation zone, and quickly calculate MWA temperature distribution. The creation of this model is a good base to improve the clinical applications of MWA.

The FEM simulation results have been proved to be in good agreement with the *ex vivo* experiment. However, in *ex vivo* experiments, the temperature of the water pumped through the simulated blood vessel was 15 °C, which was different from the body temperature (37 °C). In order to explore the different cooling effects of cold water on MWA simulations, the temperature of simulated blood in the model was properly changed. In the condition of the vessel diameter of 6 mm and the vessel-antenna spacing of 10 mm, water temperatures were set to 15 °C, 20 °C, 25 °C, 30 ° C, 35 °C and 37 °C, respectively. It was found that changing the water temperature would not have a significant effect on the shape of the coagulation zone, but would affect the volume of the final coagulation zone. When the water temperature rose from 15 °C to 37 °C, the volume of the final coagulation zone increased by about 7.3%. For every 5 °C rise, the volume would increase by about 1.6%. In addition, for the temperature distribution, two groups of experiments at 15 °C and 37 °C were compared and the temperature differences were calculated. The average value (mean P_i) of these differences was used to represent the influences of the water temperature on MWA result at a specified point. It was found that the temperature measurement

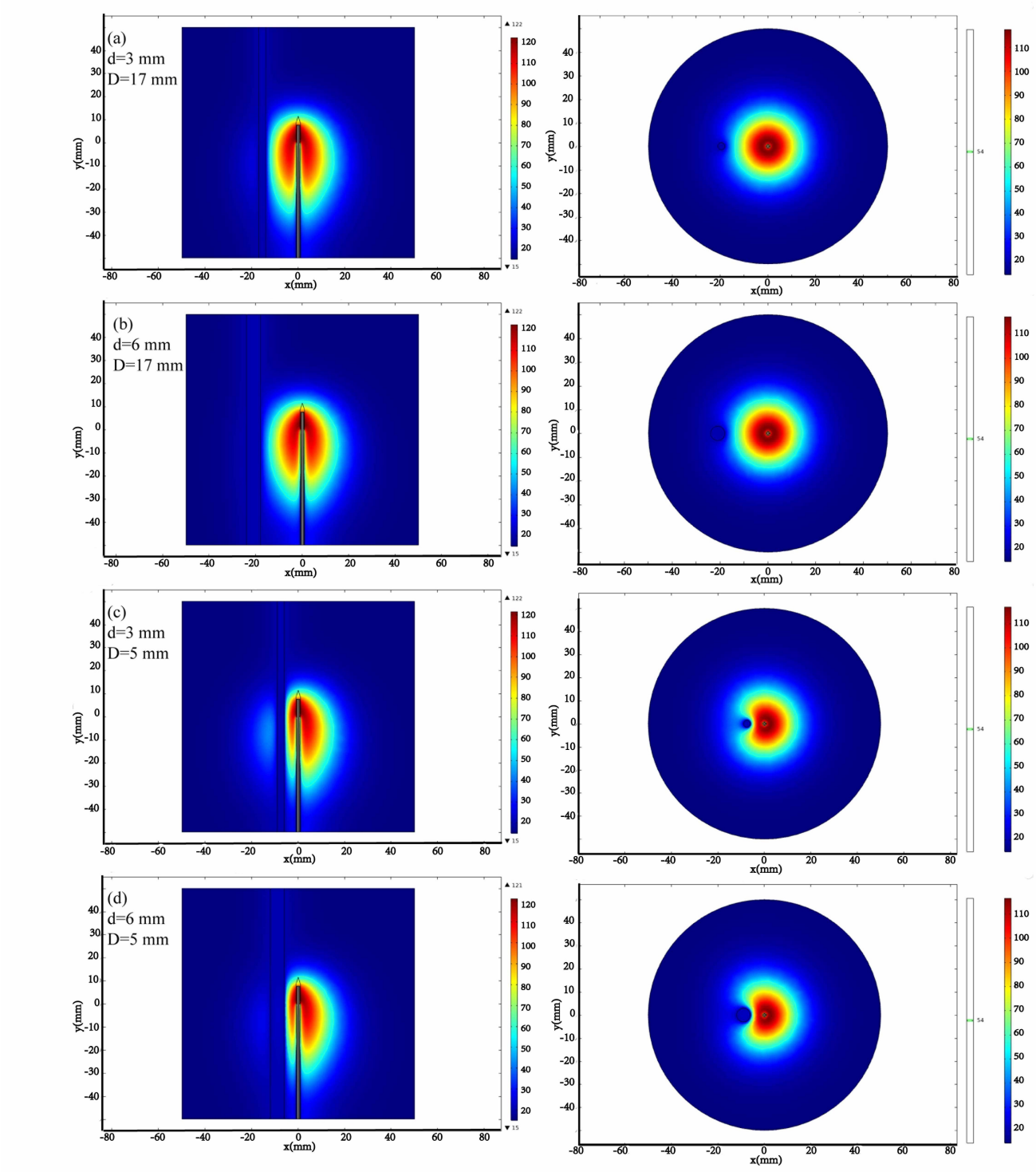

Fig. 7. Simulation temperature profiles of vessels with diameters of 3 mm and 6 mm at spacings of 5 mm and 17 mm (d stands for the vessel diameter, D stands for the vessel-antenna spacing and the blood flow rate was 2.0 m/s). (a) and (b) had the same vessel-antenna spacing of 17 mm, and the vessel diameter in (a) and (b) was 3 mm and 6 mm, respectively. (c) and (d) had the same vessel-antenna spacing of 5 mm, and the vessel diameter in (c) and (d) was 3 mm and 6 mm, respectively.

points near the antenna could hardly be affected by the simulated blood temperature (mean $P_4 = 0.55$, mean $P_6 = 0.58$). However, the point near the blood vessel would be obviously impacted (mean $P_1 = 1.56$). This was because the cooling effect of cold water was stronger and the heat sink effect was more obvious.

Through the finite element simulation, the influences of blood (d $\geq$3 mm) flow parameters on MWA tem-

Table 4. The temperature difference for vessel diameters of 3 mm and 6 mm when the vessel-antenna spacing was 5 mm.

	P_1 [95% CI*]	P_4 [95% CI*]	P_6 [95% CI*]
Mean temperature difference during first 10 s	0.69 [0.52–0.87]	0.27 [0.10–0.44]	0.21 [0.10–0.44]
Temperature difference at 360 s	2.11	1.02	1.32

*95% CI denotes Confidence interval at 95% confidence level.

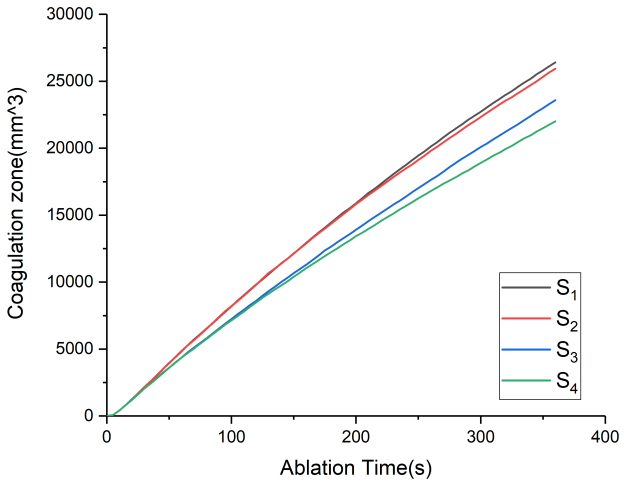

Fig. 8. Variation of coagulation volume with time (S_1, S_2, S_3 and S_4 represent four groups of simulations under different conditions. S_1: d = 3 mm, D = 17 mm; S_2: d = 6 mm, D = 17 mm; S_3: d = 3 mm, D = 5 mm; S_4: d = 6 mm, D = 5 mm. d stands for the vessel diameter, D stands for the vessel-antenna spacing and the blood flow rate was 2.0 m/s.).

perature distribution were obtained. In the case of small vessels, the coagulation effect caused by heating and the directional effect of blood flow are significant. Not just like small vessels, in the study of large vessels, the coagulation zone will not be formed on the lateral side of the vessel during ablation. In was found in this study that the cooling effects of large blood vessels could protect the vessel wall from damage and prevent blood coagulation near the heated zone, and will not produce directional effects. This is beneficial in that there are no needs for clinicians to monitor the local temperature of the vessel wall [15], which makes the operation more convenient.

This study systematically analyzes the influences of single large vessel around tumor on microwave temperature distribution. It was observed that the cooling effects were obvious on the side of large vessels. Compared with the opposite side without the blood vessels, the temperature rise rate of this side was slower, and the temperature of tissue during MWA was also lower. In the early stage of MWA, there were no significant temperature differences under different blood flow conditions. As the ablation time went on, obvious temperature differences appeared. At the end of ablation, the temperature differences reached the maximum. For the temperature measurement point close to the large vessel (such as P_1), the critical time of significant temperature difference could occur earlier. This was because the temperature distribution was affected faster by thermal diffusion effect at a location proximate to large vessel.

In addition, the results show that the vessel-antenna spacing possesses a greater influence on the temperature distribution than the vessel diameter. On the other hand, the presence of a vessel with larger diameter and smaller vessel-antenna spacing will make the volume of the coagulation zone significantly decrease. However, the vessel-antenna spacing greater than the short half-axis of the predicted coagulation zone will not contribute to the considerable changes of the coagulation zone (the average change is only 1.2%). In RFA, the electrical conductivity change caused by vessel cooling effect will increase the coagulation zone [35]. However, MWA is not sensitive to the heat-sink effect. Once the big vessel does not overlap with the predicted coagulation zone, it will hardly have an obvious impact on the simulation results. In a further investigation on the coagulation zone characterization, if the vessel-antenna spacing exceeds the short half axis of the coagulation zone, the characteristic length growth model [41] can be used to characterize coagulation zone. Otherwise, it is necessary to derive vessel influence factor based on vessel contributions. This factor in combination with the characteristic length growth model may be used to characterize the coagulation zone. In this way, more accurate model of the coagulation zone can be provided for clinicians.

One of the disadvantages of this study is that because the porcine liver tissue is very elastic, it is hard to accurately place the thermocouples. Secondly, porcine livers are histologically different from human livers in that they have more connective tissue, which might influence MWA temperature distribution. According to Vaidya [11], directional effects on the coagulation zone were found to occur for blood vessel radii between 0.4 mm and 0.5 mm. Huang [10] found that, the directional effect occur for small blood vessels (irrespective of flow rate) or large vessels with low flow rate. Because this study focuses on the normal blood flow rate of human body, the direction and velocity of blood flow in large vessels are not considered. In the simulation process, in order to simulate the cooling effects of large vessels *ex vivo* experiment, the convection heat transfer equation was used to describe the cooling effects of blood heating on tissue. In order to further improve the accuracy of simulation, the setting of convection heat transfer coefficient needs further studied. In addition, *ex vivo* experiments are limited in their expressiveness compared to *in vivo* ap-

proaches. In a further investigation, the *ex vivo* liver and simulated blood can be left at 37 °C for a period of time until their temperatures are consistent with the body temperature. In this way, the experimental results will be closer to the *in vivo* situations.

6. Conclusions

A temperature simulation model on MWA was established by appropriately setting the blood flow parameters. The effectiveness of the model was verified by *ex vivo* experiments. Both the vessel-antenna spacing and the diameter of large vessel will affect the temperature distribution and the volume of coagulation zone. The vessel-antenna spacing is the more significant factor, and the diameter of vessel is much less significant. The cooling effects of large vessels does not work in the early stage of MWA (0–10 s). Since microwave ablation is not sensitive to heat sink effect, the volume of coagulation zone will not be significantly affected when the vessel falls outside the predicted coagulation zone. This study can provide a more practical reference for tumor MWA under conditions simulating an *in vivo* setting and can improve the accuracy of preoperative planning.

7. Author contributions

HG and SH designed the study. SW and ZW conducted the experiment. JW analyzed the data. JW and HG wrote the paper. All authors have read and approved the final manuscript.

8. Ethics approval and consent to participate

Not applicable.

9. Acknowledgment

The authors would like to thank the anonymous reviewers for their constructive comments and suggestions.

10. Funding

This work was supported by the National Natural Science Foundation of China (Grant Nos. 61871005 and 82171941).

11. Conflict of interest

The authors declare no conflict of interest.

12. References

[1] Singh S, Melnik R. Thermal ablation of biological tissues in disease treatment: a review of computational models and future directions. Electromagnetic Biology and Medicine. 2020; 39: 49–88.

[2] Wright AS, Mahvi DM, Haemmerich DG, Lee FT. Minimally invasive approaches in management of hepatic tumors. Surgical Technology International. 2003; 11: 144–153.

[3] Fagnoni FF. Combination of radiofrequency ablation and immunotherapy. Frontiers in Bioscience (Landmark Edition). 2008; 13: 369.

[4] Keisari Y. Tumor abolition and antitumor immune stimulation by physico-chemical tumor ablation. Frontiers in Bioscience (Landmark Edition). 2017; 22: 310–347.

[5] Hariharan P, Chang I, Myers MR, Banerjee RK. Radiofrequency ablation in a realistic reconstructed hepatic tissue. Journal of Biomechanical Engineering. 2007; 129: 354–364.

[6] Lopresto V, Pinto R, Farina L, Cavagnaro M. Treatment planning in microwave thermal ablation: clinical gaps and recent research advances. International Journal of Hyperthermia. 2017; 33: 83–100.

[7] Radosevic A, Prieto D, Burdío F, Berjano E, Prakash P, Trujillo M. Short pulsed microwave ablation: computer modeling and ex vivo experiments. International Journal of Hyperthermia. 2021; 38: 409–420.

[8] Brace CL. Microwave Ablation Technology: what every User should know. Current Problems in Diagnostic Radiology. 2009; 38: 61–67.

[9] Ahmed M, Brace CL, Lee FT, Goldberg SN. Principles of and advances in percutaneous ablation. Radiology. 2011; 258: 351–369.

[10] Huang H. Influence of blood vessel on the thermal lesion formation during radiofrequency ablation for liver tumors. Medical Physics. 2013; 40: 073303.

[11] Vaidya N, Baragona M, Lavezzo V, Maessen R, Veroy K. Simulation study of the cooling effect of blood vessels and blood coagulation in hepatic radio-frequency ablation. International Journal of Hyperthermia. 2021; 38: 95–104.

[12] Chen R, Lu F, Wu F, Jiang T, Xie L, Kong D. An analytical solution for temperature distributions in hepatic radiofrequency ablation incorporating the heat-sink effect of large vessels. Physics in Medicine and Biology. 2018; 63: 235026.

[13] Lu Y, Nan Q, Du J, Li L, Qiao A, Liu Y. Experimental study on thermal field in the vicinity of arterial bifurcation in microwave ablation therapy. International Journal of Hyperthermia. 2010; 26: 316–326.

[14] Chen X, Saidel GM. Mathematical modeling of thermal ablation in tissue surrounding a large vessel. Journal of Biomechanical Engineering. 2009; 131: 011001.

[15] Lu DS, Raman SS, Vodopich DJ, Wang M, Sayre J, Lassman C. Effect of vessel size on creation of hepatic radiofrequency lesions in porcine: Assessment of the 'heat sink' effect. American Journal of Roentgenology. 2002; 178: 47–51.

[16] Shih T, Liu H, Horng AT. Cooling effect of thermally significant blood vessels in perfused tumor tissue during thermal therapy. International Communications in Heat and Mass Transfer. 2006; 33: 135–141.

[17] Haemmerich D, Staelin T, Tungjitkusolmun S, Lee FT, Mahvi DM, Webster JG. Hepatic bipolar radio-frequency ablation between separated multiprong electrodes. IEEE Transactions on Biomedical Engineering. 2001; 48: 1145–1152.

[18] Arkin H, Xu LX, Holmes KR. Recent developments in modeling heat transfer in blood perfused tissues. IEEE Transactions on Bio-Medical Engineering. 1994; 41: 97–107.

[19] Pennes HH. Analysis of tissue and arterial blood temperature in the resting human forearm. Applied Physiology. 1948; 1: 93–122.

[20] Van Leeuwen GM, Kotte AN, Raaymakers BW, Lagendijk JJ. Temperature simulations in tissue with a realistic computer- generated vessel network. Physics in Medicine and Biology. 2000; 45: 1035–1049.
[21] Consiglieri L, Santos ID, Haemmerich D. Theoretical analysis of the heat convention coefficient in large vessels and the significance for thermal ablative therapies. Physics in Medical and Biology. 2003; 48: 4125–4134.
[22] Nakayama A, Kuwahara F. A general bioheat transfer model based on the theory of porous media. International Journal of Heat and Mass Transfer. 2008; 51: 3190–3199.
[23] Haemmerich D, Wright AW, Mahvi DM, Lee FT, Webster JG. Hepatic bipolar radiofrequency ablation creates coagulation zones close to blood vessels: a finite element study. Medical & Biological Engineering & Computing. 2003; 41: 317–323.
[24] Yu J, Liang P, Yu X, Liu F, Chen L, Wang Y. A comparison of microwave ablation and bipolar radiofrequency ablation both with an internally cooled probe: results in ex vivo and in vivo porcine livers. European Journal of Radiology. 2011; 79: 124–130.
[25] Gao H, Wang X, Wu S, Zhou Z, Bai Y. 2450-MHz microwave ablation temperature simulation using temperature-dependence feedback of characteristic parameters. International Journal of RF and Microwave Computer-Aided Engineering. 2019; 29: e21488.
[26] Gao H, Wang X, Wu S, Zhou Z, Bai Y, Wu W. Conformal coverage of liver tumors by the thermal coagulation zone in 2450-MHz microwave ablation. International Journal of Hyperthermia. 2019; 36: 590–604.
[27] Ji Z, Brace CL. Expanded modeling of temperature-dependent dielectric properties for microwave thermal ablation. Physics in Medicine and Biology. 2011; 56: 5249–5264.
[28] Lopresto V, Pinto R, Cavagnaro M. Experimental characterization of the thermal lesion induced by microwave ablation. International Journal of Hyperthermia. 2014; 30: 110–118.
[29] Cavagnaro M, Pinto R, Lopresto V. Numerical models to evaluate the temperature increase induced by *ex vivo* microwave thermal ablation. Physics in Medical and Biology. 2015; 60: 3287–3311.
[30] Yang D, Converse MC, Mahvi DM, Webster JG. Expanding the Bioheat Equation to Include Tissue Internal Water Evaporation during Heating. IEEE Transactions on Biomedical Engineering. 2007; 54: 1382–1388.
[31] Rossmanna C, Haemmerich D. Review of temperature dependence of thermal properties, dielectric properties, and perfusion of biological tissues at hyperthermic and ablation temperatures. Critical Reviews in Biomedical Engineering. 2014; 42: 467–492.
[32] Ahmed M, Solbiati L, Brace CL, Breen DJ, Callstrom MR, Charboneau JW, *et al*. Image-guided tumor ablation: standardization of terminology and reporting criteria-A 10-year update. Journal of Vascular and Interventional Radiology. 2014; 25: 1691–705.e4.
[33] Sun Y, Cheng Z, Dong L, Zhang G, Wang Y, Liang P. Comparison of temperature curve and ablation zone between 915- and 2450-MHz cooled-shaft microwave antenna: results in *ex vivo* porcine livers. European Journal of Radiology. 2012; 81: 553–557.
[34] Ai H, Wu S, Gao H, Zhao L, Yang C, Zeng Y. Temperature distribution analysis of tissue water vaporization during microwave ablation: experiments and simulations. International Journal of Hyperthermia. 2012; 28: 674–685.
[35] Poch FGM, Rieder C, Ballhausen H, Knappe V, Ritz J, Gemeinhardt O, *et al*. The vascular cooling effect in hepatic multipolar radiofrequency ablation leads to incomplete ablation *ex vivo*. International Journal of Hyperthermia. 2016; 32: 749–756.
[36] Pohlan J, Kress W, Hermann K, Mews J, Kroes M, Hamm B, *et al*. Computed Tomography Thermography for Ablation Zone Prediction in Microwave Ablation and Cryoablation: Advantages and Challenges in an *Ex Vivo* Porcine Liver Model. Journal of Computer Assisted Tomography. 2020; 44: 744–749.
[37] Arthur RM, Straube WL, Trobaugh JW, Moros EG. Noninvasive estimation of hyperthermia temperatures with ultrasound. International Journal of Hyperthermia. 2005; 21: 589–600.
[38] Pernot M, Tanter M, Bercoff J, Waters KR, Fink M. Temperature estimation using ultrasonic spatial compound imaging. IEEE Transactions on Ultrasonics, Ferroelectrics, and Frequency Control. 2004; 51: 606–615.
[39] Zhou Y. Noninvasive Thermometry in High-Intensity Focused Ultrasound Ablation. Ultrasound Quarterly. 2017; 33: 253–260.
[40] Quesson B, de Zwart JA, Moonen CT. Magnetic resonance temperature imaging for guidance of thermotherapy. Journal of Magnetic Resonance Imaging. 2000; 12: 525–533.
[41] Gao H, Wang X, Wu S, Zhou Z, Bai Y, Ai H. Characterization of 2450-MHz microwave thermal coagulation zone based on characteristic length growth model and shape variation factor. International Journal of RF and Microwave Computer-Aided Engineering. 2019; 29: e21705.

Abbreviations: MWA, Microwave Ablation; RFA, Radiofrequency Ablation; SAR, Specific Absorption Rate; 3D, three-dimensional; FEM, Finite Element Method.

Keywords: Liver tumor; Microwave ablation; Temperature distribution; Simulation model

Send correspondence to:

Hongjian Gao, Faculty of Environmental and Life Sciences, Beijing University of Technology, 100124 Beijing, China, E-mail: gaohongjian@bjut.edu.cn

Shengyang Huang, Faculty of Environmental and Life Sciences, Beijing University of Technology, 100124 Beijing, China, E-mail: hsy@bjut.edu.cn